ALCHEMY : JOURNAL OF CHEMISTRY

Research Article

Targeting AKT1 in Oral Cancer: *In Silico* Insights from *Chrysanthemum morifolium* Phytoconstituents

F. S. Haris[1], S. T. Damayanti[1], Prisca Valensia[1], N. M. Mardiana[1], S. R. Aziz[1], F. A. Anjani[1], Dhania Novitasari[2]*

[1]Bachelor Program in Pharmacy, Faculty of Pharmacy, Universitas Padjadjaran, Sumedang, 45363, West Java, Indonesia
[2]Department of Pharmaceutical Analysis and Medicinal Chemistry, Faculty of Pharmacy, Universitas Padjadjaran, Sumedang, 45363, West Java, Indonesia

ARTICLE INFO

Article History
Received: 09 July 2026
Revised: 5 September 2026
Accepted: 22 September 2026
Available online: 30 October 2026

* Email (Author Correspondence): dhania@unpad.ac.id

DOI: https://doi.org/10.18860/al.v14i2.44929

ABSTRACT

Oral squamous cell carcinoma (OSCC) is a prevalent type of oral cancer known to be closely associated with the activation of the PI3K/AKT/mTOR pathway, particularly the AKT1 protein, which plays a critical role in cancer cell proliferation, migration, and survival. This study aims to evaluate the potential of bioactive compounds from Chrysanthemum flowers (*Chrysanthemum morifolium*) as AKT1 inhibitor candidates using an *in silico* approach. A total of 30 bioactive compounds were then analyzed through drug-likeness assessment based on Lipinski's rule, ADME-Tox prediction, pharmacophore screening, and molecular docking against the AKT1 receptor (PDB ID: 3CQW). The results revealed that 17 out of 30 compounds complied with Lipinski's rule, while all compounds were successfully identified as hits in the best pharmacophore model with an AUC value of 0.70. Molecular docking for the compounds then were validated using the protein's original ligand, yielding a reliable RMSD value of 0.76 Å. Apigenin-7-O-glucuronide exhibited the highest pharmacophore fit score of 34.42, whereas apigenin-7-O-glucoside demonstrated the best binding affinity with a binding energy of -10.29 kcal/mol, which was lower than the reference compound Capivasertib (-9.52 kcal/mol). However, based on the integration of all evaluated parameters, apigenin exhibited the most balanced profile, characterized by compliance with Lipinski's rule, favorable ADME-Tox properties, a pharmacophore fit score of 34.22, and the lowest inhibition constant value of 0.00193 µM. Collectively, apigenin holds strong potential as a promising AKT1 inhibitor candidate for the development of OSCC therapeutics and warrants further investigation through *in vitro* and *in vivo* studies.

Keywords: Oral squamous cell carcinoma, AKT1, *Chrysanthemum morifolium*, pharmacophore screening, molecular docking.

1. Introduction

Cancer is one of the leading degenerative diseases with a high mortality rate worldwide. According to the Global Cancer Observatory (GLOBOCAN), approximately 19 million new cancer cases were reported globally in 2022, and this number continues to rise. Of these cases, around 9 million resulted in death. In Indonesia, more than 408,661 new cancer cases and nearly 242,099 cancer-related deaths were recorded in 2022. Among the various types of cancer, oral cancer represents a significant public health concern. Oral Squamous Cell Carcinoma (OSCC) is the most common type of oral cancer. In Indonesia, oral cancer ranks as the 14th most prevalent cancer, with approximately 6,515 new cases reported annually and about 3,500 deaths recorded in 2022 [1].

Oral squamous cell carcinoma (OSCC) develops through a multistep process involving the accumulation of genetic alterations and disruption of the tumor microenvironment. Chronic exposure to various risk factors induces deoxyribonucleic acid (DNA) damage and mutations in genes regulating cell growth, resulting in oncogene activation and tumor suppressor gene inactivation [2]. These alterations lead to the loss of regulatory control over cell proliferation, differentiation, apoptosis, angiogenesis, and tissue invasion. Consequently, normal oral epithelial cells progressively transform into precancerous lesions and eventually develop into invasive carcinoma capable of metastasizing to regional lymph nodes and distant organs, including the lungs, liver, and bones [3].

One of the major molecular pathways involved in OSCC progression is the PI3K/AKT/mTOR signaling pathway. Under normal physiological conditions, this pathway regulates essential cellular processes, including cell growth, proliferation, metabolism, and survival [4]. The pathway is activated when growth factors, such as epidermal growth factor (EGF), bind to receptor tyrosine kinases (RTKs) on the cell membrane, thereby activating phosphoinositide 3-kinase (PI3K). Activated PI3K converts phosphatidylinositol 4,5-bisphosphate (PIP2) into phosphatidylinositol 3,4,5-trisphosphate (PIP3), which recruits and activates AKT through phosphorylation by phosphoinositide-dependent kinase-1 (PDK1) and the mammalian target of rapamycin complex 2 (mTORC2) [2]. Activated AKT subsequently regulates several downstream proteins, including mTOR, nuclear factor kappa B (NF-κB), and glycogen synthase kinase-3 beta (GSK3β), to maintain the balance between cell proliferation and programmed cell death [5].

AKT is a serine/threonine protein kinase comprising three isoforms: AKT1, AKT2, and AKT3. Among these isoforms, AKT1 plays the predominant role in regulating cell proliferation and survival. In normal cells, AKT1 activation is tightly controlled and occurs only in response to appropriate extracellular stimuli. However, in cancer cells, including OSCC, this regulatory mechanism is disrupted due to mutations, gene amplification, or overexpression of components within the PI3K/AKT/mTOR pathway, leading to constitutive AKT1 activation [6]. Persistent AKT1 activation promotes cell proliferation, protein synthesis, and resistance to apoptosis, thereby facilitating tumor growth and progression [7]. Therefore, inhibition of AKT1 has emerged as a promising therapeutic strategy for suppressing uncontrolled cell proliferation and serves as an attractive molecular target for the development of novel anticancer agents.

In the search for potential anticancer agents, chrysanthemum (*Chrysanthemum sp.*) has emerged as a promising natural source. This plant, commonly known as seruni or golden flower in Indonesia, is widely cultivated as an ornamental plant and consumed as an herbal beverage. It has also been traditionally used for medicinal purposes. In addition to its traditional applications, Chrysanthemum species have demonstrated potential as a source of anticancer compounds. Their therapeutic properties are attributed to the presence of diverse secondary metabolites, particularly phenolic acids and flavonoids [8]. Okanin, a chalcone compound isolated from Chrysanthemum species, has demonstrated anticancer activity through the activation of caspase-3. Caspase-3 activation induces both apoptosis and pyroptosis. Furthermore, okanin inhibits cancer cell proliferation by inducing G2/M phase cell cycle arrest and reducing the proliferative capacity of cancer cells [9]. Considering the diversity of bioactive compounds present in Chrysanthemum species, further investigation is warranted to identify additional compounds with potential anticancer activity against OSCC. These compounds may target specific molecular proteins involved in OSCC progression. Among these targets, AKT1, a central regulator of the PI3K/AKT/mTOR signaling pathway, represents a promising therapeutic target for the development of targeted therapies against OSCC.

From a structural perspective, the AKT1 kinase domain contains an ATP-binding pocket located within the cleft between the N-and C-terminal lobes. This pocket comprises several conserved structural elements, including the glycine-rich loop, the αC-helix, and the hinge region [10]. The hinge residues Glu228 and Ala230 contribute to the recognition and stabilization of ATP and ATP-competitive inhibitors through hydrogen-bond interactions [10], [11]. The presence of polar residues within the hinge region, together with hydrophobic and aromatic residues surrounding the ATP-binding cavity, provides multiple interaction sites for small-molecule ligands. These structural characteristics provide a rationale for investigating flavonoids as

potential AKT1 inhibitors. The characteristic C6–C3–C6 flavonoid scaffold contains two aromatic rings and a heterocyclic ring bearing hydroxyl and carbonyl functional groups, which can provide complementary hydrophobic, π-mediated, and hydrogen-bond interactions with residues within protein kinase binding pockets. Previous studies have demonstrated that flavonoids can interact with the ATP-binding sites of several protein kinases, including AKT1, through combinations of hydrogen bonding and hydrophobic or aromatic interactions [12].

Therefore, this study aims to identify and evaluate the potential of bioactive compounds derived from Chrysanthemum species as candidate anticancer agents against OSCC using an in silico approach. Using in silico approach for analyzing potential anticancer compounds will enable the use of molecular docking to predict the binding affinity and interaction between bioactive compounds and the target protein AKT1. Furthermore, in silico predictions can provide preliminary information regarding the physicochemical properties of the compounds, such as drug-likeness, absorption, distribution, metabolism, excretion, toxicity, and potential biological activities of the identified compounds. The in silico method can also serve as a more efficient strategy for screening potential compound candidates and identifying the most promising candidates for further experimental investigation. The evaluation will involve analyzing the interactions between the compounds and the AKT1 receptor, comparing their binding characteristics with those of a reference anticancer compound, and assessing their predicted pharmacokinetic properties and biological activities. The findings of this study are expected to identify potential AKT1 inhibitors and contribute to the development of natural product-based therapeutic strategies for the treatment of OSCC.

2. Materials and Methods

2.1. *Materials*

Thirty compounds from *Chrysanthemum morifolium* selected as potential anticancer candidates in this study were identified based on the work of Peng *et al* [8]. Based on their work, they characterized various phenolic compounds and other secondary metabolites to evaluate their protective effects against oxidative stress-induced erythrocyte damage. These 30 compounds will then be individually evaluated against the target receptor to assess their binding affinity and physicochemical properties for this research.

The computational simulation conducted in this study involved several software packages and databases. ChemDraw Ultra 12.0 and Chem3D Pro 12.0 were used for ligand structure modeling and energy minimization. Molecular docking was performed using AutoDock 4.2, while docking preparation and visualization were carried out using BIOVIA Discovery Studio 2025. Ligand-based pharmacophore models were generated using LigandScout 4.4.5.

The target macromolecular structure used in this study was the AKT1 protein (PDB ID: 3CQW), obtained from the Protein Data Bank (PDB). The test ligands consisted of 30 compounds isolated from *Chrysanthemum morifolium*, whose chemical structures were retrieved from the PubChem database and previously reported to possess biological activities [8]. The molecular docking protocol was validated using the Directory of Useful Decoys, Enhanced (DUD-E) database. Finally, physicochemical properties and ADMET (absorption, distribution, metabolism, excretion, and toxicity) profiles based on Lipinski's Rule of Five were evaluated using the SwissADME web server (*https://www.swissadme.ch/*) and the pkCSM web server (*https://biosig.lab.uq.edu.au/pkcsm*), respectively.

2.2. *Methods*

2.2.1 *Lipinski's Rule of Five*

The physicochemical characteristics of the test compounds were evaluated based on Lipinski's Rule of Five criteria using the SwissADME platform. The procedure was initiated by retrieving the chemical structure of each target ligand from the PubChem database. The SMILES code of each compound was copied and entered into the ligand input field on the official SwissADME website (https://www.swissadme.ch). After executing the analysis by clicking the Run button, the output data, including molecular weight, lipophilicity (LogP), hydrogen bond donor, and hydrogen bond acceptor capacities, were analyzed to determine the drug-likeness profile of each compound and subsequently recorded systematically [13].

2.2.2 *ADME-Tox*

The pharmacological properties of the test compounds were evaluated to predict their safety and efficacy profiles in the body based on the parameters of absorption, distribution, metabolism, excretion, and toxicity (ADME-Tox) using the pkCSM web server. The SMILES codes of the compounds were obtained from the PubChem database and pasted into the input field on the pkCSM website (*https://biosig.lab.uq.edu.au/pkcsm*). The analysis was performed by selecting the ADMET option and allowing the prediction process to complete. The obtained parameters included human intestinal absorption (HIA, %), Caco-2 permeability (nm/s), fraction unbound (fu), blood-brain barrier (BBB) permeability, CYP2D6 substrate, CYP3A4 substrate, renal OCT2 substrate, total clearance, AMES toxicity, and hepatotoxicity [14].

2.2.3 *Pharmacophore Screening*

Pharmacophore screening was performed using LigandScout. Active compounds and decoy datasets were obtained from the Directory of Useful Decoys, Enhanced (DUD-E), imported into the Ligand-Based Perspective, and saved in .ldb format. The test compounds were then imported individually and assigned as the Test type.

Pharmacophore model generation was initiated by loading the active compound database, followed by energy minimization and clustering. One representative compound from each cluster was selected as the training set to generate 1–10 pharmacophore models, which were subsequently saved in .pmz format. The generated models were validated using the active compound and decoy datasets through the Screening Perspective feature. Model performance was evaluated based on the area under the receiver operating characteristic curve (AUC), where a model with an AUC value of at least 0.70 was considered acceptable. The best-performing model was subsequently used for virtual screening of the test compounds. The screening results identified hit compounds, defined as compounds possessing pharmacophoric features that matched those of the native ligand interacting with the target receptor [13].

2.2.4 *Molecular Docking*

Molecular docking was performed using AutoDock 4.2 and BIOVIA Discovery Studio. The target protein structure AKT1 was obtained from the RCSB Protein Data Bank with a PDB ID of 3CQW and a resolution of 2.00 Å and prepared in the AutoDock 4.2. The receptor was prepared by separating the protein from the inhibitor and substrate peptide, while the native inhibitor was retained separately for subsequent redocking validation. All crystallographic water molecules were removed from the receptor structure, and non-essential non-protein molecules were excluded before docking. Hydrogen atoms were added to the receptor, and the protonation states of ionizable amino acid residues were assigned to represent the physiological pH condition. Partial atomic charges were subsequently assigned using the charge scheme implemented. Method validation was carried out through redocking of the native ligand using the Lamarckian Genetic Algorithm with 100 runs and was considered successful when the root mean square deviation (RMSD) was less than 2.0 Å. The test compounds and reference compounds were prepared from SMILES structures obtained from PubChem, energy-minimized using the MM2 method in Chem3D, and docked into the active site of the receptor using the same docking parameters applied during the validation process. The docking space for the ligand was prepared using a grid box with a dimension of 40 in every axis (x,y,z), and the resolution was set to 0.375 Å. Docking results were analyzed based on binding energy, inhibition constant (Ki), and amino acid residue interaction profiles through two-dimensional (2D) and three-dimensional (3D) visualization using BIOVIA Discovery Studio [13].

3. Results and Discussion

This study evaluates the potential of phytochemical compounds from Chrysanthemum flowers (*Chrysanthemum morifolium*) as AKT1 inhibitors through a computational approach. The methods applied include Lipinski's rule-based drug-likeness assessment, ADME-Tox profile prediction, pharmacophore screening, and molecular docking. This combined approach aims to select potential compounds that possess favorable pharmacokinetic properties and low toxicity levels, while simultaneously exhibiting strong binding affinity toward the target receptor.

The selection of AKT1 as the target receptor in this study is based on its extensive role in various types of cancer, as well as its proven specific association with OSCC, a prevalent type of oral cancer [7]. Activation of this receptor involves phosphorylation at the T308 residue by PDK1 and the S473 residue by mTORC2. This process subsequently inhibits downstream substrates such as GSK3, TSC2, caspase 9, PRAS40, and FOXO1 through phosphorylation, thereby suppressing apoptosis and promoting uncontrolled cell growth [15]. Immunohistochemical examination of OSCC tissues confirmed that positive cytoplasmic p-AKT expression was found in approximately 94.2% of samples. This high accumulation of p-AKT demonstrates that the AKT protein pathway is actively involved in this oral malignancy [4].

3.1. *Lipinski's Rule of Five*

Lipinski's Rule of Five sets specific criteria for drug-likeness, which include a molecular weight below 500 Da, a LogP value of no more than 5 for lipophilicity, and a maximum of 5 hydrogen bond donors and 10 hydrogen bond acceptors [16].

Table 1. Drug-likeness prediction results based on Lipinski's Rule of Five

No.	Compounds	Molecular Weight (Da)	Log P	Hydrogen Bonds		Result
				Donor	Acceptor	
1.	Okanin	288.25	1.69	5	6	P
2.	Luteolin	288.24	1.73	4	6	P
3.	Quercetin	30224	1.23	5	7	P
4.	Apigenin	270.24	2.11	3	5	P
5.	Diosmetin	300.26	2.19	3	6	P
6.	Maritimetin	286.24	2.56	6	4	P
7.	Chlorogenic Acid	354.31	-0.39	6	9	P
8.	Isookanin	288.25	1.37	4	6	P
9.	Acacetin	284.26	2.52	2	5	P
10.	Butein	272.25	1.96	4	5	P
11.	Eriodictyol	288.25	1.45	4	6	P
12.	Sulfuretin	270.24	1.90	3	5	P
13.	Naringenin	272.25	1.84	3	5	P
14.	Taxifolin	304.25	0.51	5	7	P
15.	Marein	450.39	-0.23	8	11	P
16.	Coreopsin	434.39	0.32	7	10	P
17.	4,5-Dicaffeoylquinic acid	516.45	0.79	7	12	NP
18.	Butin	272.25	1.66	3	5	NP
19.	Linarin	592.55	-0.25	7	14	NP
20.	Rutin	610.52	-1.51	10	16	NP
21.	Luteolin-7-O-glucoside	448.38	0.15	7	11	NP
22.	Luteolin-7-O-glucoronide	462.36	-0.06	7	12	NP
23.	Apigenin-7-O-glucoside	578.52	1.93	6	12	NP
24.	Apigenin-7-O-glucoronide	446.36	0.17	6	11	NP
25.	Diosmetin-7-O-glucoside	462.40	0.57	6	11	NP
26.	4,5-Dicaffeoylquinic acid	516.45	0.80	7	12	NP
27.	Maritimetin-6-O-glucoside	448.38	-0.21	7	11	NP
28.	Naringenin-7-O-glucoside	434.39	0.10	6	10	P
29.	Eriodictyol-7-O-glucoside	450.39	-0.32	7	11	NP
30.	Eriodictyol-7-O-glucuronide	464.38	-0.22	7	12	NP

Note:
P: Passed with 0 to 1 violation
NP: Not Passed with more than 1 violation

Evaluating the drug-likeness of bioactive compounds from Chrysanthemum flowers using Lipinski's Rule of Five provides crucial insights into their potential as orally active drugs in humans. The screening indicated that a majority of the

analyzed compounds successfully passed the criteria (**Table 1**). This passing group mainly consists of flavonoid aglycones, chlorogenic acid, and specific glycoside structures. These molecules display a well-balanced profile between hydrophilic and lipophilic properties, which is essential for predicting their ability to passively cross biological membranes and be effectively absorbed through the gastrointestinal tract. Even though certain glycoside structures possess molecular weights approaching the upper threshold due to their sugar moieties, they still passed all parameters since Lipinski's rule tolerates a single violation without completely compromising oral pharmacokinetic potential.

Conversely, the remaining compounds failed to meet the criteria due to multiple parameter violations (**Table 1**). These non-passing molecules are generally heavier flavonoid glycosides or highly polar derivatives. The attachment of multiple sugar units increases both the molecular size and the number of hydrogen bond acceptors well beyond the permissible limits. Biophysically, this high polarity and large molecular volume significantly impede the ability of these compounds to penetrate lipid bilayers via passive diffusion, consequently reducing their predicted oral bioavailability. Overall, this evaluation demonstrates that while heavy glycosides face natural permeation barriers, the high proportion of passing aglycones indicates that Chrysanthemum flowers represent a promising source of structurally sound candidates for further therapeutic development.

3.2. *ADME-Tox*

ADME-Tox prediction evaluates five key pharmacokinetic parameters to assess how well a compound is absorbed by the body, how it is distributed throughout biological tissues, how long it remains in the body, and its potential safety risks. Accordingly, ADME-Tox is a computational approach used to predict the absorption, distribution, metabolism, excretion, and toxicity properties of drug candidates. Absorption evaluates the extent to which a compound can be absorbed into the body, distribution assesses its ability to reach and disperse throughout tissues, metabolism predicts how efficiently the compound is biotransformed by metabolic enzymes, excretion estimates how readily it can be eliminated from the body, and toxicity evaluates its potential to produce harmful effects.

Table 2. Pharmacokinetic and toxicity profile of candidate compounds based on ADME-Tox prediction

No.	Compounds	Absorption		Distribution		Metabolism		Excretion		Toxicity	
		HIA (%)	Caco-2 (nm/sec)	Fraction Unbound	BBB	CYP2D6 substrate	CYP3A4 substrate	Renal OCT2 substrate	Total clearance (log mL/min/kg)	AMES Toxicity	Hepato-toxicity
1	Okanin	57.71	-0.45	0.30	-1.23	×	×	×	-0.14	×	×
2	Luteolin	81.13	0.10	0.17	-0.91	×	×	×	0.50	×	×
3	Quercetin	77.21	-0.23	0.21	-1.10	×	×	×	0.41	×	×
4	Apigenin	93.25	1.01	0.15	-0.73	×	×	×	0.57	×	×
5	Diosmetin	79.90	0.37	0.09	-0.95	×	×	×	0.60	×	×
6	Maritimetin	76.07	0.75	0.13	-1.12	×	×	×	-0.12	✓	×
7	Chlorogenic acid	36.38	-0.84	0.66	-1.41	×	×	×	0.31	×	×
8	Isookanin	82.59	1.41	0.16	-1.20	×	×	×	-0.01	✓	×
9	Acacetin	94.32	1.14	0.08	-0.20	×	✓	×	0.66	×	×
10	Butein	72.57	-0.02	0.23	-0.90	×	×	×	0.02	×	×
11	Eriodictyol	74.69	-0.09	0.11	-0.83	×	×	×	-0.01	×	×

12	Sulfuretin	91.65	1.01	0.08	-0.94	×	×	×	-0.01	✓	×
13	Naringenin	91.31	1.03	0.06	-0.58	×	×	×	0.06	×	×
14	Taxifolin	64.71	0.92	0.32	-0.73	×	×	×	-0.08	×	×
15	Marein	28.64	-1.16	0.33	-1.48	×	×	×	-0.17	×	×
16	Coreopsin	35.38	0.06	0.29	-1.29	×	×	×	-0.01	×	×
17	3,5-Dicaffeoylquinic acid	47.29	-1.08	0.28	-1.97	×	✓	×	0.06	×	×
18	Butin	93.17	1.17	0.12	-0.75	×	×	×	-0.01	×	×
19	Linarin	36.68	0.36	0.12	-1.64	×	×	×	0.10	×	×
20	Rutin	23.45	-0.95	0.19	-1.90	×	×	×	-0.37	×	×
21	Luteolin-7-O-glucoside	37.56	0.25	0.22	-1.56	×	×	×	0.48	×	×
22	Luteolin-7-O-glucuronide	15.20	-0.89	0.30	-1.48	×	×	×	0.52	×	×
23	Apigenin-7-O-glucoside	37.61	0.33	0.22	-1.39	×	×	×	0.55	×	×
24	Apigenin-7-O-glucuronide	15.26	-0.69	0.31	-1.31	×	×	×	0.59	×	×
25	Diosmetin-7-O-glucoside	36.26	0.37	0.12	-1.62	×	×	×	0.58	×	×
26	4,5-Dicaffeoylquinic acid	29.04	-1.20	0.29	-2.08	×	✓	×	-0.04	×	×
27	Maritimetin-6-O-glucoside	44.71	0.23	0.25	-1.39	×	×	×	-0.22	×	×
28	Naringenin-7-O-glucoside	36.04	0.42	0.19	-1.26	×	×	×	0.38	×	×
29	Eriodictyol-7-O-glucoside	30.66	0.32	0.23	-1.51	×	×	×	0.05	×	×
30	Eriodictyol-7-O-glucuronide	5.40	-0.79	0.31	-1.43	×	×	×	-0.04	×	×

Note:
✓: indicates a positive prediction (yes)
×: indicates a negative prediction (no)

ADME-Tox prediction was performed to evaluate the pharmacokinetic profile and safety of bioactive compounds from *Chrysanthemum morifolium*. The predicted ADME parameters included gastrointestinal absorption, cellular permeability, plasma protein binding affinity, and blood–brain barrier (BBB) permeability (**Table 2**). Toxicity assessment was also conducted computationally by predicting the mutagenic and hepatotoxicity potential of the compounds. The predicted human intestinal absorption (HIA) values showed considerable variation among the tested compounds. Compounds such as acacetin, sulfuretin, diosmetin, apigenin, naringenin, butin, maritimetin, and butein exhibited high HIA values (>80%), indicating favorable oral absorption. These compounds generally possessed relatively low molecular weights and optimal lipophilicity, facilitating their diffusion across the intestinal lipid membrane. In contrast, the remaining compounds exhibited HIA values ranging from 2.86% to 79.43%. Most of these compounds contained glycosidic moieties that increased the number of oxygen atoms, resulting in higher polarity and larger molecular size. Excessive polarity and increased molecular size may hinder passive diffusion across the intestinal lipid membrane [17].

The Caco-2 permeability parameter was also used to predict the intestinal absorption of orally administered compounds. Caco-2 permeability is classified as low (<4 nm/s), moderate (4–70 nm/s), or high (>70 nm/s) [18]. Among the 30 bioactive compounds from *Chrysanthemum morifolium*, quercetin (3.41 nm/s) and taxifolin (3.42

nm/s) exhibited low permeability. Low Caco-2 permeability suggests limited membrane transport due to factors such as molecular size, polarity, or the tendency of a compound to act as a substrate for cellular efflux transporters. The remaining 28 compounds showed moderate permeability, with values ranging from 4.53 to 19.53 nm/s, indicating an adequate ability to permeate the intestinal epithelial barrier.

For the distribution profile, the fraction unbound (fu) parameter was used to estimate the proportion of a compound that remains unbound to plasma proteins and is therefore available to reach its therapeutic target. An fu value greater than 0.2 was considered favorable because compounds with fu values below 0.2 may experience up to a twofold increase in the free drug fraction under altered physiological conditions, potentially leading to unpredictable pharmacological responses and an increased risk of adverse effects [19]. Sixteen compounds exhibited fu values above 0.2, ranging from 0.206 to 0.658. Higher fu values indicate a greater proportion of free drugs in plasma, which may enhance tissue distribution and pharmacodynamic activity but may also result in more rapid elimination [7]. Conversely, lower fu values are generally associated with higher lipophilicity, leading to stronger plasma protein binding that prolongs systemic retention but reduces the fraction of drug available to interact directly with the therapeutic target [20].

Another distribution parameter evaluated was blood–brain barrier (BBB) permeability, which predicts the ability of a compound to penetrate the blood–brain barrier. All tested compounds exhibited BBB values below 2.0, indicating low to moderate BBB permeability. This suggests limited distribution into the central nervous system. For AKT1 inhibitors intended for the treatment of non-central nervous system cancers, limited BBB penetration may be advantageous because it reduces the risk of neurological adverse effects while maintaining therapeutic activity in peripheral tissues [19].

The metabolism profile was evaluated based on the likelihood of compounds being metabolized by cytochrome P450 (CYP450) enzymes. The parameters assessed included CYP2D6 substrate and CYP3A4 substrate predictions, which indicate whether a compound can be metabolized by the corresponding enzymes. Compounds identified as CYP substrates are expected to undergo enzymatic metabolism, potentially influencing their plasma concentration and duration of action. These parameters also provide an indication of possible drug-to-drug interactions when compounds sharing the same metabolic pathway are co-administered [21]. The prediction results showed that three compounds: acacetin, 3,5-dicaffeoylquinic acid, and 4,5-dicaffeoylquinic acid, were predicted to be CYP3A4 substrates, whereas none of the tested compounds were predicted to be CYP2D6 substrates.

The excretion profile was evaluated using renal OCT2 substrate and total clearance parameters. The renal OCT2 substrate parameter predicts whether a compound is transported by the organic cation transporter 2 (OCT2), which mediates renal secretion from the bloodstream into the kidneys for urinary excretion. Total clearance reflects the overall efficiency of the body in eliminating a compound through all elimination pathways. Higher total clearance values indicate faster elimination, whereas lower values suggest prolonged systemic exposure [22]. All tested compounds were predicted to be non-substrates of renal OCT2, indicating that OCT2-mediated renal transport is unlikely to contribute significantly to their elimination. Total clearance values ranged from −0.369 to 0.663 log mL/min/kg. Acacetin exhibited the highest total clearance (0.663 log mL/min/kg), suggesting relatively rapid elimination, whereas rutin showed the lowest value (−0.369 log mL/min/kg), indicating slower elimination and potentially prolonged systemic circulation.

The toxicity profile included predictions of AMES toxicity and hepatotoxicity. AMES toxicity predicts the mutagenic potential of a compound, whereas hepatotoxicity estimates its potential to induce liver toxicity, one of the major safety concerns in drug development. Both parameters are reported as either "Yes" or "No." A "Yes" result for AMES toxicity indicates potential mutagenicity, whereas a "Yes" result for hepatotoxicity suggests a risk of liver toxicity. Therefore, a "No" prediction for both parameters is considered desirable, indicating a favorable safety profile [23]. Based on the prediction results, three compounds: maritimetin, isookain, and sulfuretin, were predicted to be AMES positive, whereas none of the tested compounds were predicted to be hepatotoxic.

Notably, apigenin demonstrated an ADME-Tox profile that supports its selection as the leading candidate. Apigenin exhibited a human intestinal absorption (HIA) value of 93.25%, indicating a high predicted intestinal absorption. In addition, apigenin was not predicted to be a substrate of CYP2D6, CYP3A4, or renal OCT2, and showed negative predictions for AMES toxicity and hepatotoxicity. These results indicate that apigenin possesses relatively favorable predicted absorption and metabolic characteristics and does not show predicted genotoxicity or hepatotoxicity based on the models used. Thus, the ADME-Tox results provide additional support for the selection

of apigenin as an AKT1 inhibitor candidate, together with the molecular docking and pharmacophore screening results. However, all ADME-Tox parameters are based on computational predictions and therefore cannot be considered definitive evidence of the pharmacokinetic and safety profiles of apigenin and still require validation through experimental studies.

3.3. *Pharmacophore Screening*

The pharmacophore model was evaluated to determine its ability to discriminate between active compounds and decoy compounds. Model validation was performed using the Receiver Operating Characteristic (ROC) curve, and its performance was assessed based on the Area Under the Curve (AUC) value. The AUC value serves as a parameter for evaluating the predictive performance of the pharmacophore model. A higher AUC value indicates a greater ability of the model to accurately identify compounds with potential activity against the target protein. Based on the validation results, Model 1 was selected as the optimal pharmacophore model, with 97 true positives (TP) and 354 false positives (FP).

Following pharmacophore validation, pharmacophore-based virtual screening was performed on all compounds in the selected database. This step aimed to identify compounds that matched the essential pharmacophore features required for interaction with the target protein. Compounds that satisfied the screening criteria were subsequently ranked according to their pharmacophore fit score, which reflects the degree of correspondence between the compounds' pharmacophoric features and the validated pharmacophore model.

Table 3. *Pharmacophore fit score*

No.	Compound	*Fit Score*
1	Apigenin-7-O-glucoronide	34.32
2	Luteolin	34.26
3	Diosmetin-7-O-glucoside	34.23
4	Eriodictyol-7-O-glucoside	34.23
5	Luteolin-7-O-glucoronide	34.22
6	Apigenin	34.22
7	Diosmetin	34.22
8	Acacetin	34.22
9	Quercetin	34.20
10	Naringenin-7-O-glucoside	34.19

Pharmacophore screening was performed to identify compounds possessing key pharmacophoric features that contribute to inhibitory activity against AKT1. In this study, a total of 30 compounds identified from *Chrysanthemum morifolium* were evaluated to identify potential hit compounds. The screening process was initiated by constructing ten pharmacophore models based on the selected set of compounds. The selection criteria employed during pharmacophore screening utilized a “fit score”, which measures the geometric alignment of molecular features with the established pharmacophore model. The highest fit scores indicate a better match to the model. The table above (**Table 3**) presents the ten candidate compounds that achieved the highest fit scores among others. Based on these values, the listed candidates demonstrate excellent compatibility, reflecting their ability to match the structural and functional features essential to the biological activity of the pharmacophore model [24].

The Area Under the Curve (AUC) values are classified as follows:

- 0,90 – 1,00 = Excellent Classification
- 0,80 – 0,90 = Good Classification
- 0,70 – 0,80 = Fair Classification
- 0,60 – 0,70 = Poor Classification
- 0,50 – 0,60 = Failure

Based on the AUC classification, models 1, 6, and 7 were considered acceptable, each exhibiting an Area Under the Curve (AUC) value of 0.7, which falls within the fair classification category. These results indicate that the generated pharmacophore queries possess adequate discriminatory ability to distinguish active compounds from decoy compounds and are therefore suitable for virtual screening of the test compounds. The three models were further evaluated based on the numbers of true positives (TP), false positives (FP), and AUC values at 1%, 5%, and 10% to determine the optimal model. Among them, Model 1 demonstrated the best overall performance, with 97 true positives, 354 false positives, and AUC values of 1.00 at the 1%, 5%, and 10% levels (**Figure 1a**).

Based on the virtual screening results using Model 1, all 30 compounds were identified as hit compounds, indicating that they possessed pharmacophoric features consistent with those required for AKT1 inhibition. Among these compounds, apigenin-7-O-glucuronide achieved the highest pharmacophore fit score (34.32), indicating the greatest degree of conformity with the selected pharmacophore model. Pharmacophore feature analysis revealed that the hit compounds shared the same essential features as the reference ligand, including one aromatic ring feature (yellow), one hydrogen bond acceptor feature (red), and one hydrogen bond donor feature (green). These pharmacological properties have important roles in mediating interactions with the target protein.

Although apigenin-7-O-glucuronide exhibited the highest pharmacophore fit score of 34.32, the fit score does not directly indicate a higher inhibitory potential. The pharmacophore fit score reflects the degree of matching between the chemical features of the ligand and the pharmacophore model but does not fully represent the energetic strength of ligand–protein interactions or the pharmacokinetic characteristics of the compound. Apigenin exhibited a fit score of 34.22, which still indicates a high degree of fit to the pharmacophore model. In addition, apigenin fulfilled the key pharmacophore features, namely an aromatic ring, hydrogen bond donor, and hydrogen bond acceptor (**Figure 1b**), which are also present in the reference ligand. Therefore, the pharmacophore screening results were considered as one of the supporting parameters rather than the sole basis for selecting the final candidate.

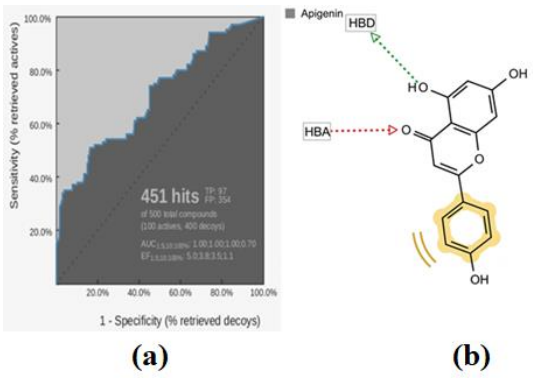


Figure 1. Results of pharmacophore screening model 1: (a) ROC validation curve; (b) Interaction with the top-ranked ligand

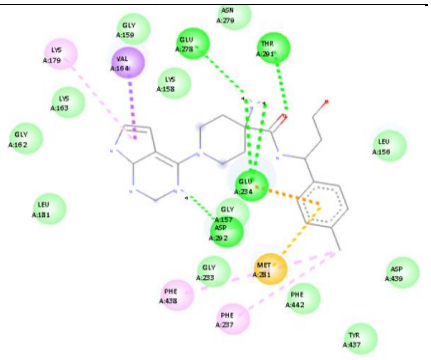
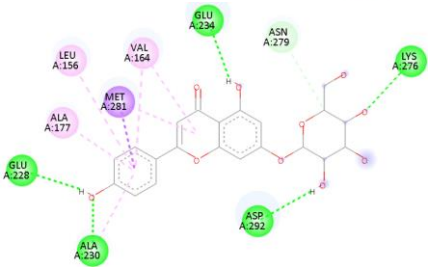
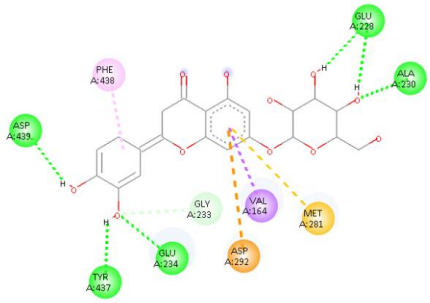
3.4. *Molecular Docking*

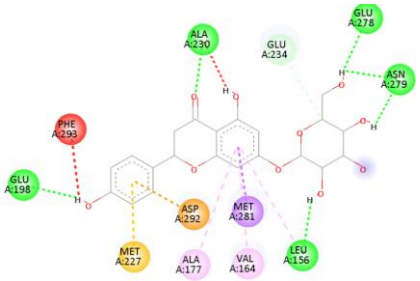
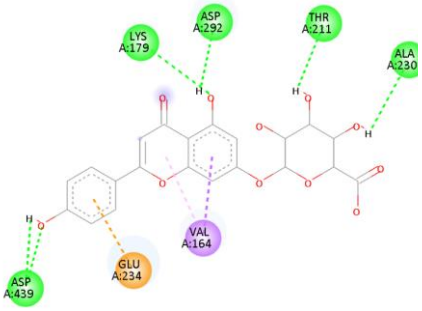
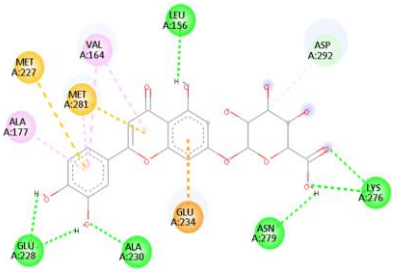
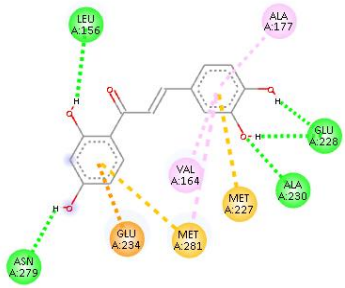
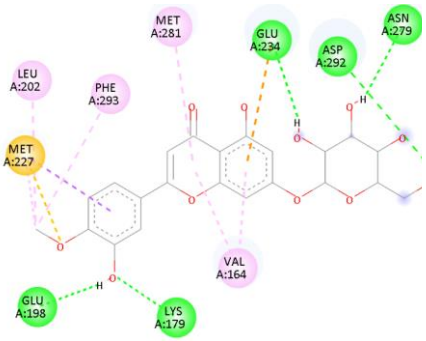
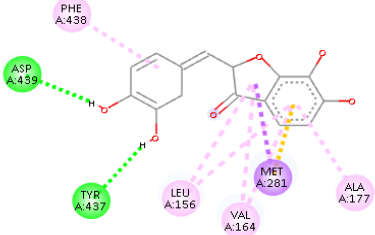
Molecular docking results were initiated by the construction of the receptor–ligand complex and overlay visualization. This process provided a comparison between the native ligand obtained from the receptor used in the study and the ligand generated through the redocking procedure. The comparison of these two ligands was used to assess the success of the method validation. The similarity between the two ligands was evaluated quantitatively

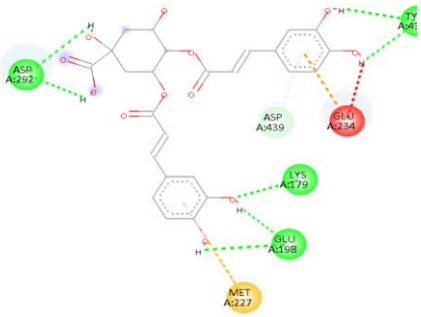
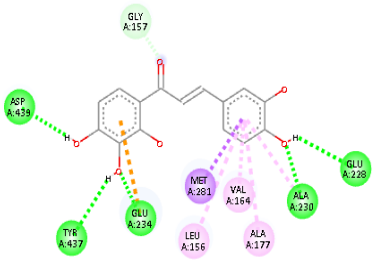
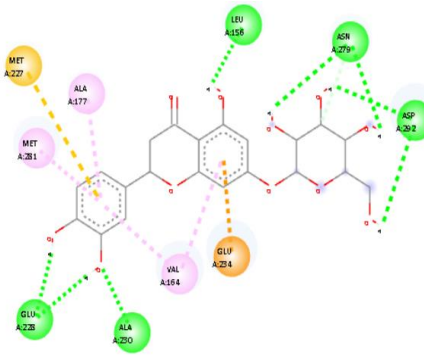
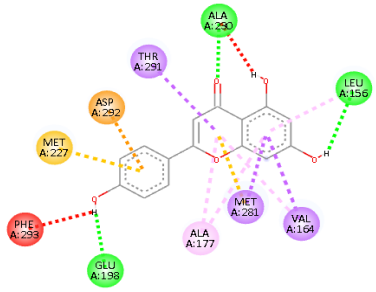
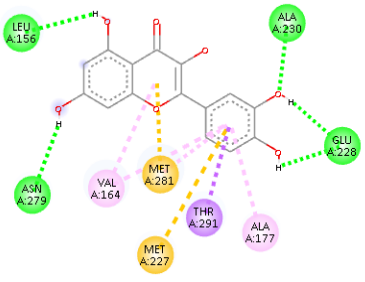
using the Root Mean Square Deviation (RMSD) value. An RMSD value of less than 2.0 Å is generally considered indicative of a valid docking method, with lower RMSD values reflecting higher accuracy of the docking protocol. A high degree of similarity between the redocked ligand and the native ligand, as indicated by an RMSD value of 0.76 Å, demonstrates that the validation was successful and that the docking protocol can be considered valid.

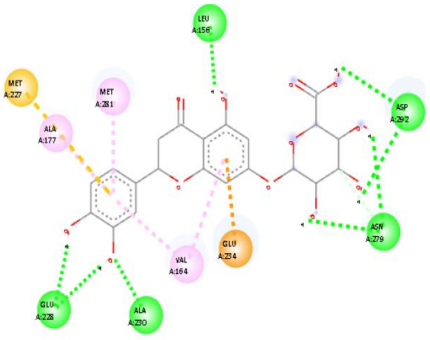
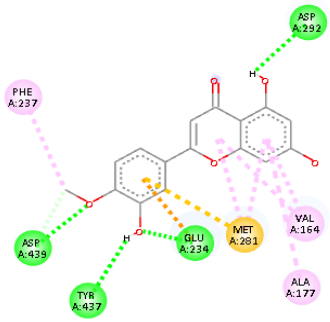
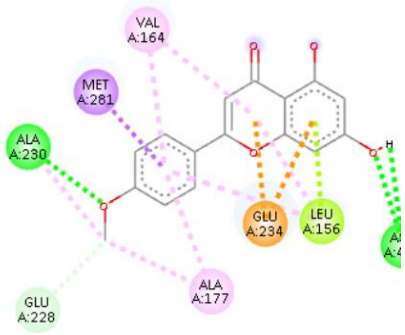
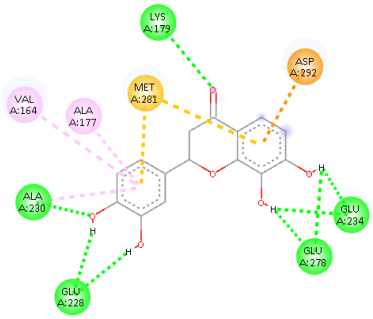
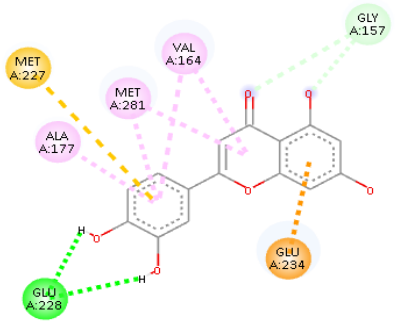
Following method validation, molecular docking was performed for the test compounds and the reference compound. This process generated the top-ranked binding conformation for each receptor–ligand complex. The resulting docking conformations provided cluster RMSD values along with their corresponding comparisons. In addition, the docking analysis yielded binding energy values and inhibition constants (Ki). Lower binding energy and Ki values indicate more favorable docking results. A more negative binding energy reflects stronger and more stable interactions between the ligand and the receptor while requiring less energy for binding. Likewise, a lower Ki indicates greater inhibitory potency, meaning that a lower concentration of the compound is required to effectively inhibit the target receptor.

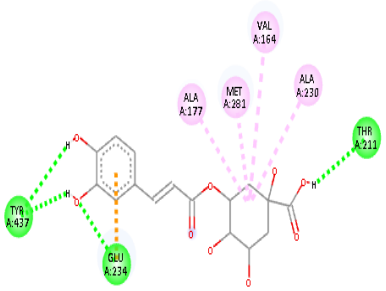
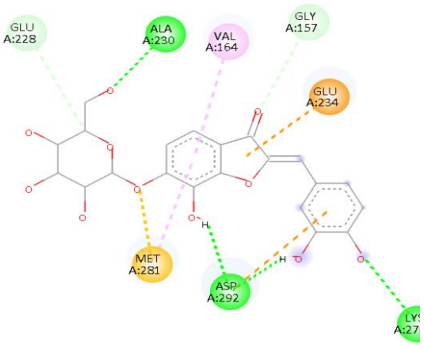
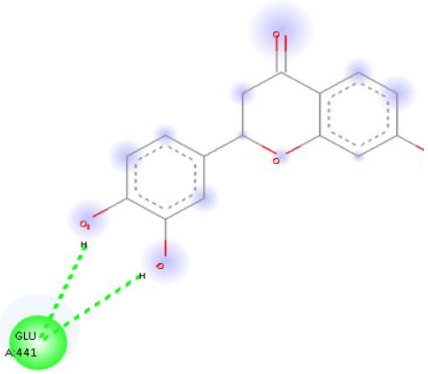
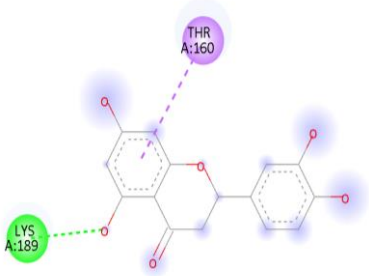
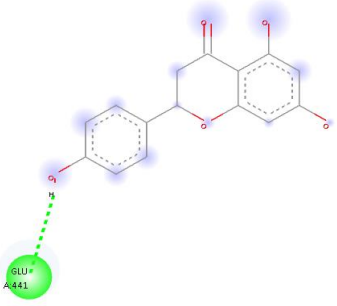
Table 4. Molecular docking results of the test compounds

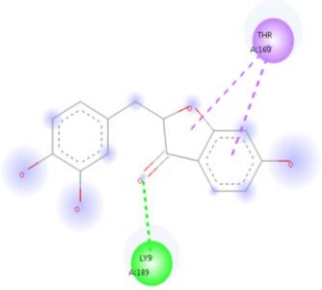
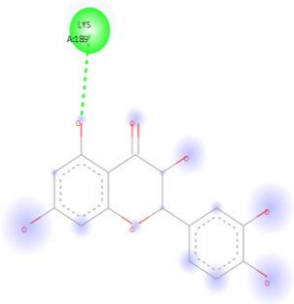
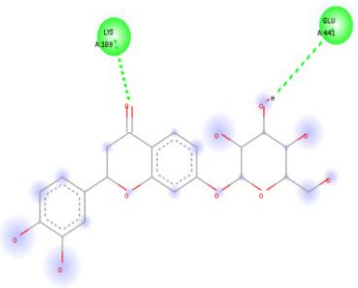
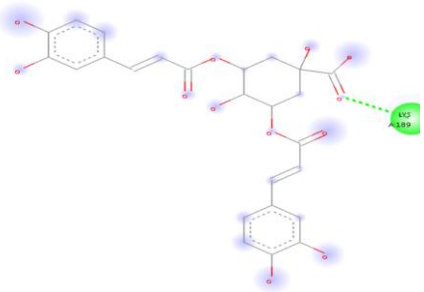
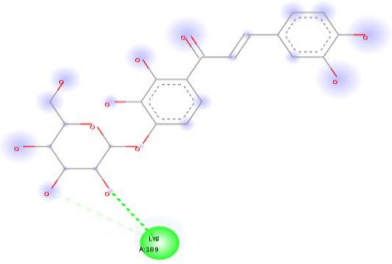
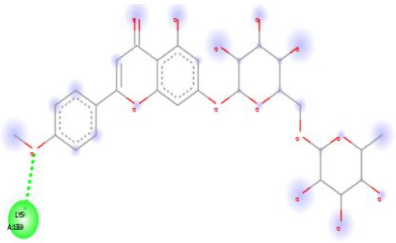
No.	Compound	Binding Energy (kcal/mol)	Inhibition Constant (μM)	2D Visualization
I	Capivasertib (reference compound)	-9.52	0.11	
1.	Apigenin-7-O-glucoside	-10.29	0.03	
2.	Luteolin-7-O-glucoside	-10.12	not available	

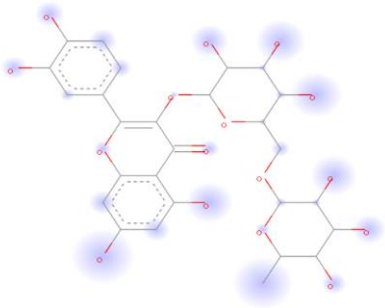
3.	Naringenin-7-O-glucoside	-9.62	0.09	
4.	Apigenin-7-O-glucuronide	-9.29	0.16	
5.	Luteolin-7-O-glucuronide	-8.76	0.38	
6.	Butein	-8.71	0.41	
7.	Diosmetin-7-O-glucoside	-8.51	0.58	
8.	Maritimetin	-8.47	0.62	

9.	4,5-Dicaffeoylquinic acid	-8.46	0.63	
10.	Okanin	-8.28	0.85	
11.	Eriodictyol-7-O-glucoside	-8.22	0.94	
12.	Apigenin	-7.80	0.00	
13.	Quercetin	-7.66	0.00	

14.	Eriodictyol-7-O-glucuronide	-7.64	2.50	
15.	Diosmetin	-7.63	0.00	
16.	Acacetin	-7.49	3.22	
17.	Isookanin	-7.42	3.66	
18.	Luteolin	-7.27	0.00	

19.	Chlorogenic acid	-7.10	6.24	
20.	Maritimetin-6-O-glucoside	-6.21	28.22	
21.	Butin	-1.26	118.87	
22.	Eriodictyol	-0.97	193.74	
23.	Naringenin	-0.86	232.92	

24.	Sulfuretin	-0.84	240.69	
25.	Taxifolin	-0.60	364.82	
26.	Coreopsin	0.40	not available	
27.	3.5-Dicaffeoylquinicacid	2.19	not available	
28.	Marein	2.20	not available	
29.	Linarin	2.71	not available	

30.	Rutin	3.52	not available	

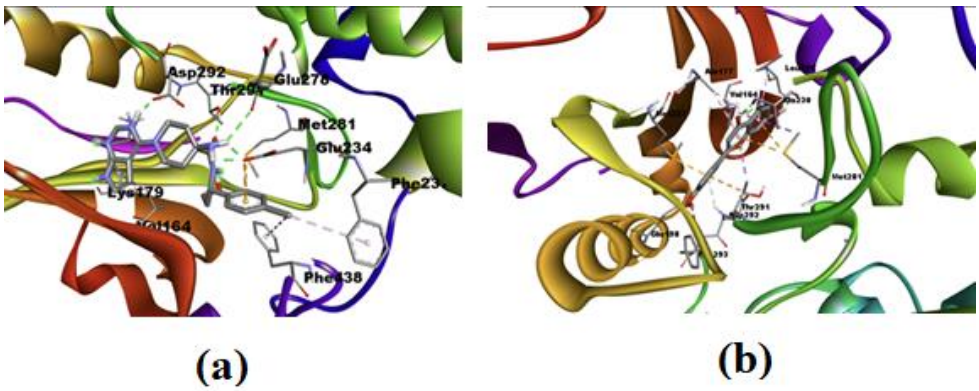


Figure 2. 3D visualization of (a) Capivarsetib; (b) Apigenin against AKT1

Molecular docking is a computational method used to predict the orientation and conformation of a ligand within the active site of a target macromolecular receptor, providing structural information on the interactions between the ligand and the receptor [26]. In this study, molecular docking was performed on 30 compounds to obtain scores generated using a scoring function (**Table 4**). A scoring function is a mathematical algorithm employed in molecular docking simulations to estimate the binding affinity or binding energy between a ligand and its receptor, while also identifying and ranking the best binding pose among all conformations generated during the docking process [27].

Before obtaining the scoring function results, an overlay visualization was performed (**Figure 3**). The overlay analysis compared the native ligand with the redocked ligand using grid coordinates of x (5.272), y (2.843), and z (18.249), resulting in an RMSD value of 0.375 Å. This value confirms the successful validation of the docking protocol, as it is below the acceptable threshold of 2.0 Å. In addition to the quantitative RMSD result, the overlay visualization demonstrated a high degree of structural and positional similarity between the native ligand and the redocked ligand, providing further evidence of the successful validation of the molecular docking method.

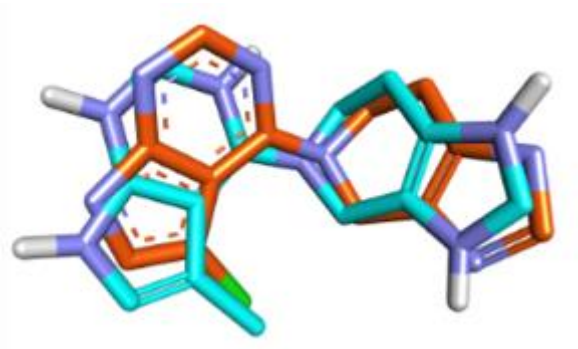


Figure 3. Overlay visualization of the redocked ligand and the native ligand

Following the overlay visualization, molecular docking was performed for the test compounds and the reference compound. This process generated scoring function results in the form of binding energy and inhibition constant (Ki) values. Capivasertib was used as the reference compound, exhibiting a binding energy of −9.52 kcal/mol and a Ki value of 0.10517 μM. Among the 30 compounds evaluated, Apigenin-7-O-glucoside showed the lowest binding energy, with a value of −10.29 kcal/mol. A more negative binding energy indicates stronger and more stable ligand–receptor interactions while requiring less energy for binding. In addition, apigenin exhibited the lowest Ki value of 0.00193 μM. A lower inhibition constant reflects greater inhibitory potency, indicating that a lower concentration of the compound is required to effectively inhibit the target receptor [28].

Molecular docking analysis revealed the amino acid residue interactions formed between the ligands and the AKT1 receptor. The reference ligand, capivasertib, established conventional hydrogen bonds, hydrophobic interactions, and π-interactions with the amino acid residues Leu156, Val164, Ala177, Met227, Met281, Asp292, as well as several neighboring residues. These interactions contribute to maintaining the ligand orientation within the ATP-binding pocket, resulting in a high binding affinity toward AKT1 [29].

It should be noted that MM2 is a classical force field method in which molecular energy is calculated based on empirically parameterized bond stretching, angle bending, torsional, and non-bonded interaction terms, without explicitly modeling the electronic structure of the molecule [30]. Consequently, atomic partial charges used in MM2-based ligand preparation rely on predefined charge parameters rather than being derived from the molecule's actual electron density. In contrast, Density Functional Theory (DFT) is a quantum mechanical method that solves the electronic structure of a molecule based on electron density functionals, thereby enabling the calculation of more accurate static partial charges, such as Mulliken or electrostatic potential (ESP)-derived charges [31]. Previous studies have shown that quantum mechanically or semi-empirically derived partial charges can improve docking geometry accuracy compared to empirical charge schemes such as Gasteiger charges [32]. Nevertheless, this improvement comes at the expense of considerably greater computational time, which limits the feasibility of DFT or large-scale virtual screening involving multiple candidate compounds. Given this trade-off, MM2 remains a practical and commonly applied method during the ligand preparation phase in numerous recent in silico anticancer and phytochemical docking studies [33], [34].

3.5. *Discussion*

Among the tested compounds, apigenin exhibited the highest similarity in interacting amino acid residues to the reference ligand, capivasertib. Apigenin interacted with Leu156, Val164, Ala177, Ala230, Met227, Met281, and Asp292, most of which are also involved in capivasertib binding. Specifically, apigenin formed conventional hydrogen bonds with Ala230 and Leu156, a π-anion interaction with Asp292, π-sulfur interactions with Met227 and Met281, π-sigma interactions with Val164 and Thr291, and π-alkyl interactions with Ala177, Leu156, Met281, and Val164. The overlap in interacting residues suggests that apigenin is capable of occupying the same ATP-binding pocket as capivasertib. However, the interaction profiles were not entirely identical. While capivasertib is primarily stabilized by an extensive hydrogen-bonding network, apigenin appears to maintain the ligand–receptor complex through a combination of hydrophobic and π-interactions. These non-covalent interactions contribute to the stability of the ligand–protein complex by strengthening the overall binding within the active site. Therefore, the similarity in binding residues between apigenin and capivasertib supports the hypothesis that apigenin may exhibit a comparable ATP-competitive binding mode toward AKT1, although with distinct interaction characteristics.

Structurally, apigenin is a flavone-class aglycone with a relatively compact flavonoid backbone and a smaller molecular size compared with its glycosylated derivatives. These characteristics may facilitate the accommodation of apigenin within the ATP-binding pocket of AKT1 and allow its aromatic and hydroxyl groups to adopt a suitable orientation for ligand–receptor interactions. Previous molecular docking studies of AKT1 have demonstrated that interactions involving hydrogen bonds, hydrophobic contacts, and π-interactions contribute to favorable ligand binding within the ATP-binding pocket, with residues such as Leu156, Val164, Ala177, Met281, and Asp292 involved in ligand recognition [35]**.** In the present study, apigenin exhibited interactions with several of these residues, supporting its ability to engage the ATP-binding pocket through a relevant interaction pattern. In contrast, the addition of a sugar moiety in glycosylated derivatives increases molecular size, the number of hydroxyl groups,

and overall polarity, which may reduce passive membrane permeability and intestinal absorption by limiting partitioning into the hydrophobic lipid bilayer. Therefore, the relatively compact and less polar structure of apigenin may provide a more favorable balance between target-site interaction and physicochemical properties compared with its glycosylated derivatives [36].

Although the lowest binding energy was observed for apigenin-7-O-glucoside, apigenin was considered a more promising AKT1 inhibitor candidate based on several other parameters. Apigenin exhibited an inhibition constant (Ki) value of 0.00193 μM, indicating a high predicted inhibitory potential compared with several other compounds. Therefore, the selection of apigenin was not based solely on its binding energy, but rather on the integration of its predicted inhibitory potential, interaction profile, and structural compatibility with the AKT1 binding pocket.

The superiority of apigenin is further supported by the pharmacophore screening results, as apigenin exhibited a pharmacophore fit score of 34.22 and satisfied the key pharmacophore features shared with the reference ligand, namely an aromatic ring, hydrogen bond acceptor, and hydrogen bond donor. Thus, although apigenin-7-O-glucoside exhibited a lower binding energy, apigenin demonstrated a more favorable balance between its target interaction capability, inhibitory potential, pharmacophore characteristics, drug-likeness, and ADME-Tox profile. Therefore, apigenin was selected as the most promising AKT1 inhibitor candidate in this study.

Based on the pharmacophore screening results obtained using Model 1, all 30 bioactive compounds from chrysanthemum flowers were identified as hit compounds, indicating that each compound possesses pharmacophore features consistent with those of AKT1 inhibitors. However, the molecular docking results revealed considerable variation among these compounds. Several compounds exhibited more negative binding energy values than the reference compound, capivasertib (−9.52 kcal/mol), whereas others produced less negative binding energy values, suggesting a reduced ability to form stable interactions with the active site of the target receptor.

Successful identification of a compound during pharmacophore screening does not necessarily guarantee strong binding affinity. Pharmacophore screening is based on matching the chemical features of a reference ligand, including aromatic ring features, hydrogen bond acceptors, and hydrogen bond donors, without comprehensively considering the energetic interactions with the target protein. Glycoside compounds generally possess high molecular weights and numerous rotatable bonds. These structural characteristics confer considerable conformational flexibility; however, upon binding within the protein's active site, the ligand loses much of its conformational freedom as it adapts to the binding pocket. This restriction in molecular motion results in an unfavorable free energy contribution, leading to less favorable binding energy values. Furthermore, chemical incompatibility between the ligand and the receptor binding pocket also contributes to reduced binding affinity. The binding pocket of AKT1 is predominantly hydrophobic, whereas compounds such as rutin and linarin contain an excess of polar functional groups. This mismatch in physicochemical properties limits the formation of optimal interactions, thereby reducing the stability and strength of the ligand–protein complex.

The core flavone scaffold of apigenin-7-O-glucoside occupies the same hydrophobic sub-pocket as apigenin while maintaining contact with Leu156, Val164, Ala177, and Met281, which form the hinge-adjacent hydrophobic wall of the AKT1 ATP-binding cleft. However, unlike apigenin, the glucosyl unit attached at the 7-O position of apigenin-7-O-glucoside extends toward the solvent-exposed rim of the pocket, where its hydroxyl groups form additional conventional hydrogen bonds with the polar/charged residues Glu228, Asn279, and Asp292. These residues have previously been reported as key anchoring points that stabilize the AKT1-ligand complex, including Lys179, Glu191, Glu228, Ala230, Glu234, and Asp292, for a potent natural-product AKT1 inhibitor [37]. Consistently, the AKT1 ATP-binding site itself has been defined in the literature to comprise Ala177, Lys179, Lys182, Ala212, Glu228, Ala230, Glu234, Glu278, Thr291, and Asp292 as the residues lining the pocket and available for hydrogen-bond or electrostatic anchoring of ATP-competitive inhibitors such as capivasertib [38]. This indicates that, rather than being purely detrimental, the sugar moiety of apigenin-7-O-glucoside can engage a secondary hydrogen-bonding subsite near the pocket entrance, generating additional enthalpic stabilization that outweighs the entropic penalty associated with the loss of rotatable-bond freedom upon finding.

This behavior differs from that of larger and more polar glycosides, such as rutin and linarin, which possess rhamnosyl-glucosyl disaccharide units. In these compounds, the extended and branched sugar chains are too large to be accommodated within the confined hydrophobic pocket while simultaneously maintaining the hydrogen-bond geometry required for stable anchoring. As a consequence, the flavone core is pushed out of optimal alignment with the hinge-region hydrophobic residues (Leu156, Val164, Ala177, Met281), resulting in steric clash and the loss

of the key hydrogen bonds that normally stabilize the aglycone scaffold, consistent with the markedly weaker binding energies and elevated inhibition constants observed for these compounds (**Table 4**). A comparable trend has been reported for flavonoid glycosides binding other enzyme pockets, where mono-glycosides retained favorable hydrogen-bonding contact between the sugar moiety and the catalytic pocket, whereas di-glycosides were found to be less active due to steric bulk, despite similar hydrogen-bonding patterns [39]. Likewise, structural analyses of hydrophobic aglycone-binding pockets lined by Phe, Val, Trp, Tyr, Met, Leu, and Ile residues have shown that such pockets can accommodate the flavone core of glucosides, provided the appended sugar does not sterically clash with the pocket walls [40].

Collectively, these residue-specific observations indicate that the binding energy of glycosylated flavonoids toward AKT1 is governed not simply by molecular size or the number of rotatable bonds, but by whether the sugar substituent can be accommodated at a polar subsite near the pocket entrance without disrupting the hydrophobic anchoring of the flavone core. In the case of apigenin-7-O-glucoside, this accommodation appears favorable, whereas in larger di-glycosides such as rutin and linarin, it is not, explaining the divergent binding energies observed among the glycoside compounds in this study.

4. Conclusion

This study identified apigenin as the most promising AKT1 inhibitor candidate among the 30 bioactive compounds from Chrysanthemum morifolium based on the integration of pharmacophore screening, molecular docking, drug-likeness, and ADME-Tox predictions. The docking protocol was successfully validated with an RMSD value of 0.76 Å, supporting the reliability of the docking analysis. Although apigenin-7-O-glucoside exhibited the most favorable binding energy (−10.29 kcal/mol) and apigenin-7-O-glucuronide showed the highest pharmacophore fit score, apigenin demonstrated the most balanced overall profile. Apigenin exhibited a high pharmacophore fit score of 34.22, a low predicted inhibition constant (Ki) of 0.00 μM, and a binding interaction pattern involving several residues also recognized by the reference ligand, capivasertib. Furthermore, its favorable Lipinski and ADME-Tox profiles support its potential drug-likeness and predicted pharmacokinetic properties. These findings suggest that apigenin may serve as a promising candidate for further development as an AKT1 inhibitor for OSCC. However, as the findings are based on computational predictions, further in vitro and in vivo studies are required to validate its inhibitory activity, molecular interactions, pharmacokinetic properties, and safety.

Acknowledgement

The authors would like to thank the Laboratory of Medicinal Chemistry, Department of Pharmaceutical Analysis and Medicinal Chemistry, Faculty of Pharmacy, Universitas Padjadjaran, for providing the facilities and technical support necessary to conduct this research.

Referencees

[1] International Agency for Research on Cancer (IARC), *Indonesia Fact Sheet, GLOBOCAN 2022*, 2024.
[2] M. Alonso-Juarranz, M. Mascaraque, E. Carrasco, T. Gracia-Cazaña, O. De La Sen, Y. Gilaberte, and F. Falahat, "The distinctive features behind the aggressiveness of oral and cutaneous squamous cell carcinomas," *Cancers*, vol. 15, no. 12, pp. 3227, 2023.
[3] Y. Tan, Z. Wang, M. Xu, B. Li, Z. Huang, S. Qin, and C. Huang, "Oral squamous cell carcinomas: State of the field and emerging directions," *International Journal of Oral Science*, vol. 15, no. 1, pp. 44, 2023.
[4] D. M. Ferreira, T. J. Neves, L. G. C. A. Lima, F. A. Alves, and M. D. Begnami, "Prognostic implications of the phosphatidylinositol 3-kinase/Akt signaling pathway in oral squamous cell carcinoma: Over expression of p-mTOR indicates an adverse prognosis," *Applied Cancer Research*, vol. 37, pp. 41, 2017.
[5] S. Lakshminarayana, D. Augustine, R. S. Rao, S. Patil, K. H. Awan, S. S. Venkatesiah, and K. Prasad, "Molecular pathways of oral cancer that predict prognosis and survival: A systematic review," *Journal of Carcinogenesis*, vol. 17, pp. 7, 2018.
[6] P. Rajendran, R. Sekar, P. S. Dhayasankar, E. M. Ali, S. A. Abdelsalam, S. Balaraman, and B. M. Abdallah,

"PI3K/AKT signaling pathway mediated autophagy in oral carcinoma: A comprehensive review," *International Journal of Medical Sciences*, vol. 21, no. 6, pp. 1165–1186, 2024.

[7] L. R. P. Queiroz, F. V. C. Barcellos, A. L. O. Costa, F. R. O. Melo, M. R. P. Lacerda, and A. L. Z. Guimaraes, "Molecular Docking and Molecules of Interest for Oral Squamous Cell Carcinoma: A Systematic Review," *Journal of Oral and Maxillofacial Surgery, Medicine, and Pathology*, vol. 37, pp. 1159–1166, 2025.

[8] A. Peng, L. Lin, M. Zhao, and B. Sun, "Classification of edible chrysanthemums based on phenolic profiles and mechanisms underlying the protective effects of characteristic phenolics on oxidatively damaged erythrocyte," *Food Research International*, vol. 123, pp. 64–74, 2019.

[9] W. T. Chia, K. Y. Chen, C. Y. Yang, C. C. Hsieh, C. H. Tsao, C. K. Lin, and Y. W. Chen, "Okanin inhibits cell growth and induces apoptosis and pyroptosis in oral cancer," *Cancers*, vol. 16, no. 18, pp. 3195, 2024.

[10] E. Primavera, D. Palazzotti, M. L. Barreca, and A. Astolfi, "Computer-Aided Identification of Kinase-Targeted Small Molecules for Cancer: A Review on AKT Protein," Pharmaceuticals, vol. 16, no. 7, pp. 993, July 2023. [Online]. Available: https://pmc.ncbi.nlm.nih.gov/articles/PMC10384952/. [Accessed Aug. 28, 2026].

[11] G. Voelcker, "Oxazaphosphorine cytostatics," Anti-Cancer Drugs, vol. 30, no. 5, pp. 435–440, June 2019. [Online]. Available: https://pmc.ncbi.nlm.nih.gov/articles/PMC9698716/. [Accessed Aug. 28, 2026].

[12] S. Safe, A. Jayaraman, R. S. Chapkin, M. Howard, K. Mohankumar, and R. Shrestha, "Flavonoids: structure–function and mechanisms of action and opportunities for drug development," Toxicological Research, vol. 37, no. 2, pp. 147–162, Jan. 2021. [Online]. Available: https://pmc.ncbi.nlm.nih.gov/articles/PMC8007671/. [Accessed Aug. 28, 2026].

[13] M. Aulia, F. Rosani, T. N. Romadhona, L. G. Kinanti, K. Gabriel, A. Rusdin, and D. Novitasari, "Catechin from Avocado Seed (*Persea americana* Mill.) Potentially Targets Estrogen Receptor-Alpha: Computational-Based Analysis," *Biota: Jurnal Ilmiah Ilmu-Ilmu Hayati*, vol. 10, no. 3, pp. 222–232, Oct. 2025

[14] N. A. Duran-Iturbide, B. I. Diaz-Eufracio, and J. L. Medina-Franco, "In Silico ADME/Tox Profiling of Natural Products: A Focus on BIOFACQUIM," *ACS Omega*, vol. 5, no. 1, pp. 16076–16084, 2020.

[15] J. S. L. Yu and W. Cui, "Proliferation, survival and metabolism: The role of PI3K/AKT/mTOR signalling in pluripotency and cell fate determination," *Development*, vol. 143, pp. 3050–3060, 2016.

[16] C. A. Lipinski, F. Lombardo, B. W. Dominy, and P. J. Feeney, "Experimental and Computational Approaches to Estimate Solubility and Permeability in Drug Discovery and Development Settings," *Advanced Drug Delivery Reviews*, vol. 46, no. 1–3, pp. 3–26, 2009.

[17] H. Zhang, Y. I. Hassan, R. Liu, L. Mats, C. Yang, C. Liu, and R. Tsao, "Molecular Mechanisms Underlying the Absorption of Aglycone and Glycosidic Flavonoids in a Caco-2 BBe1 Cell Model," *ACS Omega*, vol. 5, pp. 10782–10793, 2020

[18] P. B. Mohite and D. D. Pawar, "In silico Prioritization of Some Tetrazole Chalcones for Anticonvulsant Activity," *International Journal of PharmTech Research*, vol. 12, no. 2, pp. 155–161, 2019.

[19] A. A. Elaine, A. Nisa, N. Tahara, D. Q. Aini, and Z. Syahriar, "In Silico Study of Mangosteen Fruit (*Garcinia mangostana* L.) as Pancreatic Anticancer Against AKT Kinase," *Indonesian Journal of Biological Pharmacy*, vol. 3, no. 1, pp. 19–32, 2023.

[20] Al-Qassabi, S. P. F. Tan, P. Phonboon, A. Galetin, A. Rostami-Hodjegan, and D. Scotcher, "Facing the facts of altered plasma protein binding: Do current models correctly predict changes in fraction unbound in special populations?," *Journal of Pharmaceutical Sciences*, vol. 113, no. 6, pp. 1664–1673, 2024.

[21] A. A. Abdelwahab, M. A. Elattar, and S. A. Fawzi, "Advancing ADMET prediction for major CYP450 isoforms: Graph-based models, limitations, and future directions," *BioMedical Engineering OnLine*, vol. 24, no. 1, pp. 93, 2025.

[22] M. Noga and K. Jurowski, "ADME of Bromo-DragonFLY as an example of a new psychoactive substance (NPS): Application of in silico methods for prediction: Absorption, distribution, metabolism and excretion," *Scientific Reports*, vol. 15, no. 1, pp. 22949, 2025.

[23] S. W. Sari, A. Wilapangga, A. N. Sari, and S. Astriani, "Studi In Silico Potensi Farmakokinetik Dua Senyawa Dari Tanaman Kenaf (*Hibiscus cannabinus* L.) Untuk Prediksi Toksisitas," *Jurnal Bina Cipta Husada*, vol. 19, no. 2, pp. 70–79, 2023.

[24] Muchtaridi, M. Syahidah, H. N. Subarnas, A. Yusuf, M. Bryant, S. D. and Langer, T, "Molecular Docking and 3D-Pharmacophore Modeling to Study the Interactions of Chalcone Derivatives with Estrogen Receptor

Alpha," *Pharmaceuticals,* vol. 10, no. 4, pp. 81, 2017. [Online]. Available: https://doi.org/10.3390/ph10040081. [Accessed Aug. 28, 2026].

[25] D. T. Wilujeng, M. Fatekurohman, and I. M. Tirta, "Analisis Risiko Kredit Perbankan Menggunakan Algoritma K-Nearest Neighbor dan Nearest Weighted K-Nearest Neighbor," *Indonesian Journal of Applied Statistics*, vol. 5, no. 2, pp. 142–148, 2023.

[26] F. Stanzione, I. Gianreco, and J. C. Cole, "Use of Molecular Docking Computational Tools in Drug Discovery," *Progress in Medicinal Chemistry*, vol. 60, pp. 273–343, 2021.

[27] J. Li, A. Fu, and L. Zhang, "An Overview of Scoring Functions Used for Protein-Ligand Interactions in Molecular Docking," *Interdisciplinary Sciences: Computational Life Sciences*, vol. 11, no. 2, pp. 320–328, 2019

[28] T. Z. A. D. Putri, R. P. Findrayani, M. Isrul, and N. Lolok, "Studi Molecular Docking Senyawa Kimia dari Herba Putri Malu (*Mimosa pudica*) Terhadap Inhibisi Enzim A-Glukosidase Sebagai Antidiabetes Melitus," *Jurnal Pharmacia Mandala Waluya*, vol. 3, no. 4, pp. 225–233, 2024.

[29] K. Petsri, M. Yokoya, S. Racha, S. Thongsom, C. Thepthanee, B. Innets, Z. Z. Ei, D. Hotta, H. Zou, and P. Chanvorachote, "Novel synthetic derivative of renieramycin T right-half analog induces apoptosis and inhibits cancer stem cells via targeting the Akt signal in lung cancer cells", *International Journal of Molecular Sciences*, vol. 24, no. 6, pp. 5345, 2023.

[30] Allinger, N. L., "Conformational Analysis. 130. MM2. Hydrocarbon Force Field Utilizing V1 and V2 Torsional Terms", vol. 99, no. 25, pp. 8127-8134, 1977.

[31] Das, A., Sahu, P., and Ali, S. M., "Molecular Dynamics Simulation or the Calibration of the OPLS Force Field Using DFT Derived Partial Charges for the Screening of Alkyl Phosphate Ligands by Studying Structure, Dynamics, and Thermodynamics", *Journal of Chemical and Engineering Data*, vol. 62, 2280-2295, 2017.

[32] Bikadi, Z. and Hazai, E., "Application of the PM6 Semi-empirical Method to Modeling Proteins Enhances Docking Accuracy of AutoDock", *Journal of Cheminformatics*, vol. 1, no. 15, 2009/

[33] Hassanejad-Asl, B., Pooresmaeil, F., Azadi, S., Najafi, A., Esmaeili, A., Bagheri-Mohammadi, S., and Kazemi, B., "Computational Drug Discovery of Potential 5α-reductase Phytochemical Inhibitors and Hair Growth Promotion Using in silico Techniques", *Frontiers in Bioinformatics*, vol. 5, pp. 1570101, 2025.

[34] Babiyana, S., Balachandran, V., Thirughanasambantham, N., Viji, A., Narayana, B., and Salian, V. V., "Synthesis, Theoretical, Spectroscopic Profiles, Topological and Structure-Based Biological Activities of 2-[3-(4-chlorophenyl0)]-5-(4-(isopropyl)phenyl)-4,5-dihydro-1 H-pyrazol-1-yl-4-(4-methylphenyl)-1,3-thiazole as a Newly Synthesis of Anti-Inflammatory Agent", *Discover Chemistry*, vol. 2, no. 273, 2025

[35] L.O. Anifowose, O.K. Paimo, F.N. Adegboyega, O.M. Ogunyemi, R.O. Akano, S.F. Hammad, and M.A. Ghazy, "Molecular docking appraisal of *Dysphania ambrosioides* phytochemicals as potential inhibitor of a key triple-negative breast cancer driver gene," *In Silico Pharmacology*, vol. 11, no. 1, p. 15, 2023. [Online]. Available: https://pmc.ncbi.nlm.nih.gov/articles/PMC10267046/. [Accessed Aug. 28, 2026].

[36] M. Berga, K. Logviss, L. Lauberte, A. Paulausks, and V. Mohylyuk, "Flavonoids in the Spotlight: Bridging the Gap between Physicochemical Properties and Formulation Strategies," *Pharmaceuticals*, vol. 16, no. 10, p. 1407, 2023. [Online]. Available: https://pmc.ncbi.nlm.nih.gov/articles/PMC10610233/. [Accessed Aug. 28, 2026].

[37] Mahajan, P., Wadhwa, B., Barik, M. R., Malik, F., and Nargotra, A., "Combining Ligand- and Structure-Based in silico Methods for the Identification of Natural Product-Based Inhibitors of AKT1", *Molecular Diversity*, vol. 24, pp. 45-60, 2020.

[38] Addies, M., Ballard, P., Buttar, D., Crafter, C., Currie, G., Davies, B. R., Debreczeni, J., Dry, H., Dudley, P., Greenwood, R., Johnson, P. D., Kettle, J. G., Lane, C., Lamont, G., Leach, A., Luke, R. W. A., Morris, J., Ogilvie, D., Page, K., Pass, M., Pearson, S., and Ruston, L., "Discovery of 4-amino-N-[(1S)-1-(4-chlorophenyl)-3-hydroxypropyl]-1-(7H-pyrrolo[2,3-d]pyrimidin-4-yl)piperidine-4-carboxamide (AZD5363), an Orally Bioavailable, Potent Inhibitor of AKT Kinases", *Journal of Medicinal Chemistry*, vol. 56, no. 5, pp.2059-2073, 2013.

[39] Borges, P. H. O., Pedreiro, S., Baptista, S. J., Geraldes, C. F. G. C., Batista, M. T., Silva, M. M. C., and Figueirinha, A., "Inhibition of α-glucosidase by Flavonoids of Cymbopogon citratus (DC) Stapf", *Journal of Ethnopharmacology*, vol. 280, pp.114470, 2021.

[40] Kotik, M., Kulik, N., and Valentová, K, “Flavonoids as Aglycones in Retaining Glycosidase-Catalyzed Reactions: Prospects for Green Chemistry”, *Journal of Agricultural and Food Chemistry*, vol. 71, pp. 14890-14910, 2023.